Supplement of Geosci. Model Dev., 11, 5203–5215, 2018
https://doi.org/10.5194/gmd-11-5203-2018-supplement

Geoscientific Model Development
Open Access
EGU

Supplement of

A generic pixel-to-point comparison for simulated large-scale ecosystem properties and ground-based observations: an example from the Amazon region

Anja Rammig et al.

Correspondence to: Anja Rammig (anja.rammig@tum.de)

Supplementary Information

Methods

1) Calculating the covariance of point observations to derive σ_ε^2

The basis for estimating σ_ε^2 is a modified version of the formula that computes the variance of a given dataset, here dataset X of point variables x_i and x_j at location *i* and *j*, (Zhang and Lei Cheng, 2012):

$$\sigma_\varepsilon^2 = cov(X,X) = \frac{1}{N^2}\sum_{i}^{N}\sum_{j}^{N}\frac{1}{2}\left(x_i - x_j\right)^2 \qquad (Eq.S1)$$

where *N* is the number of observations. The advantage of equation (SI 1) is that it is based on pairs of x and does not require the mean of X. By calculating the average half-square difference of pairs of x_i and x_j at location *i* and *j* for a specified distance that corresponds to the size of a grid cell, we obtain an estimate of the average within-grid-cell variance of point observations σ_ε^2. This mathematical representation is conceptually equivalent to the nugget effect in a semivariogram. This nugget effect is interpreted as the sum of variance caused by small-scale variability and observation errors (Cressie, 1993) and is thus fully consistent with our interpretation of σ_ε^2.

2) Calculating the corrected correlation coefficient r_{corr} and the maximum achievable correlation coefficient r_{max}

The overall difference between two datasets X and Y of observed *x* and point values *y* at spatial location *i* is captured by the mean squared deviation E^2:

$$E^2 = \frac{1}{N}\sum_{i=1}^{N}(x_i - y_i)^2 \qquad (Eq.S2)$$

However, the convenience of expressing differences in a single figure comes at the cost of not being able to distinguish in which aspects (the mean, the "amplitude" meaning the variability or roughness of the pattern, or the "shape" of the spatial pattern) the two datasets differ. For this purpose, E^2 can be decomposed into different components. In the first step, the overall bias in the mean can be isolated:

$$E^2 = E'^2 + (\bar{x} - \bar{y})^2 \qquad (Eq.S3)$$

where $\bar{x}$ and $\bar{y}$ are the arithmetic means of X and Y, respectively, and E'^2 is the mean squared difference of the centred patterns defined as:

$$E'^2 = \frac{1}{N}\sum_{i=1}^{N}\left((x_i - \bar{x}) - (y_i - \bar{y})\right)^2 \qquad (Eq.S4)$$

E'^2 is related to the correlation coefficient r and the variances σ_x^2 and σ_y^2 of X and Y, respectively:

$$E'^2 = \sigma_x^2 + \sigma_y^2 - 2\sigma_x\sigma_y r \qquad (Eq.S5)$$

Eq. S5 is the underlying principle of the Taylor diagram (Taylor, 2001), in which the root-mean-square difference E', the correlation coefficient r, and differences between standard deviations σ_x and σ_y are visualized in a concise and easily recognizable way. However, the above described relationship between E' and the difference of σ_x and σ_y is ambiguous as an underestimation of standard deviation can lead to a higher or lower E', depending on the value of r. Therefore, in the following, we will focus on the variance σ_x^2 and σ_y^2 , and on the correlation coefficient r and will show the use of the Taylor diagrams below.

Similar to the variance, errors also add quadratically so that a corrected estimate of the mean squared difference E'^2 is also obtained by subtracting σ_ε^2:

$$E'^2_{corr} = E'^2 - \sigma_\varepsilon^2 \qquad (Eq.S6)$$

Thus, the root-mean-square difference E'_{corr} is always smaller than E'. Due to the quadratic relationship, the increment $E' - E'_{corr}$ is inversely related to E', i.e. the correction is stronger for smaller E'.

The quantification of the effect of σ_ε^2 on r is less obvious but can be derived by rearranging equation Eq. S5 for r:

$$r = \frac{\sigma_x^2 + \sigma_y^2 - E'^2}{2\sigma_x\sigma_y} \qquad (Eq.S7)$$

By replacing σ_x^2 with $\sigma_{x,corr}^2$ and E'^2 with E'^2_{corr} we can obtain an equation for the calculation of r_{corr}:

$$r_{corr} = \frac{\sigma_{x,corr}^2 + \sigma_y^2 - E'^2_{corr}}{2\sigma_{x,corr}\sigma_y} \qquad (Eq.S8)$$

By combining Eq. S7 and Eq. S8 we find that:

$$\frac{r_{corr}}{r} = \frac{\sigma_x}{\sigma_{x,corr}} \qquad (Eq.S9)$$

This means that r is corrected by the same factor f as σ_y/σ_x, but the implications are different. The correlation coefficient varies between +1 and -1, with +1 indicating total positive correlation, 0 indicating no linear correlation, and -1 indicating total negative correlation. Since the correction for σ_ε^2 is equivalent to multiplying with a factor $f > 1$, r_{corr} is always larger than r if r is positive and smaller if r is negative. This means that the σ_ε^2 equally affects positive and negative correlation and has no effect if X and Y are totally uncorrelated. However, the correction does not have the potential to change the sign of r. There is an upper bound for positive r and a lower bound for negative r that can be achieved for a given σ_ε^2. For the case $\sigma_{x,corr}^2 = \sigma_\varepsilon^2 = \sigma_x^2/2$, these limits are $1/\sqrt{2}$ and $-1/\sqrt{2}$, respectively.

In this way, we can also calculate a "maximum achievable correlation coefficient" r_{max}. Assume, we correlate the observed dataset vs. the observed dataset we would get a correlation coefficient r = 1. If we now correct one of these datasets by σ_ε, its correlation reduces by factor $\frac{\sigma_x}{\sigma_{x,corr}}$, which gives us r_{max} similar to Eq. SI 9 with r=1. This means that r is corrected by the same factor f as $\frac{\sigma_x}{\sigma_{x,corr}}$. Assuming that $r_{corr} = r * f$ and $\sigma_{x,corr} = \sigma_x * f$ then $= \frac{\sigma_{x,corr}}{\sigma_x}$.

With r=1, it becomes

$$r_{corr} = 1 * \frac{\sigma_{x,corr}}{\sigma_x} = r_{max} \qquad \textit{(Eq. S10)}$$

3) Description of the dynamic global vegetation models (DGVMs)

Below, we provide a short description for each of the four DGVMs applied in our study, which is taken from the Appendix S2 from Johnson et al. (2016):

ORCHIDEE

The ORCHIDEE model (Krinner et al., 2005) consists of a DGVM coupled to the SECHIBA land-surface model (Ducoudré et al., 1993). ORCHIDEE has been previously evaluated against data from flux tower sites (Verbeeck et al. 2011) and forest plot data (Delbart et al., 2010).

Photosynthesis in ORCHIDEE is simulated following the formulations of Farquhar et al. (1980) and Collatz et al. (1992), while stomatal conductance is computed via the technique of Ball et al. (1987). Maintenance respiration of plant pools in ORCHIDEE is calculated using PFT-specific functions of (a) temperature and biomass and (b) nitrogen/carbon ratios (see Ruimy et al., 1996). Soil layering characteristics are site dependent, with rooting distributions determined by availability of water, light and nitrogen. By definition, vegetation phenology is prognostic and is based on PFT-specific temperature and moisture constraints (Krinner et al. 2005). With respect to biomass pools, the model consists of four separate carbon pools, plus total soil carbon (Verbeeck et al. 2011). Representation of vegetation dynamics and disturbance follows the approach described in the LPJ model (Sitch et al., 2003). For the simulations in this study an 11 layer soil hydrology scheme was used (Guimberteau et al., 2012).

LPJmL

In LPJmL (Bondeau et al., 2007;Gerten et al., 2004;Sitch et al., 2003), most physiological and hydrological processes are simulated at daily time steps, whereas vegetation dynamics and PFT composition are updated annually. Natural vegetation is represented by nine plant functional types (PFTs) which describe the main characteristics of plants within the different biomes across the globe. Over Amazonia, the dominant PFTs are tropical evergreen trees and tropical raingreen trees. Photosynthesis is based on the Farquhar model approach (Farquhar and von Caemmerer, 1982;Farquhar et al., 1980) with air temperature and radiation controlling photosynthetic activity at the leaf level. Transpiration and photosynthesis are coupled through stomatal conductance of the leaves, where increasing transpirational losses or carbon starvation due to closed stomata can reduce NPP under drought conditions or high temperatures. With continued drought depleting soil water storage, tropical raingreen trees shed their leaves during the dry season to avoid carbon loss and mortality. Tropical evergreen broadleaf trees keep their leaves and are thus usually outcompeted in a seasonal dry tropical climate.

Carbon gained is allocated annually to the living carbon pools where basic allometric relations between crown area, tree height and stem diameter are met (Sitch et al. 2003). The pipe model ensures that each unit of leaf area is supported by a corresponding area of transport tissue, i.e. the sapwood cross-sectional area. Canopy closure is assumed but no crown overlap is permitted. Furthermore, plants can invest more carbon to fine roots under water-limited conditions to reduce drought risks This term is parameterized for each PFT.

Tree mortality results from heat stress, fire and light competition. The latter can occur due to low growth efficiency or thinning effects. Mortality from heat stress occurs when a PFT-specific temperature is crossed (Sitch et al. 2003), and individuals lost through fire are quantified by a PFT-specific parameter describing fire intensity and severity (Thonicke et al., 2001).

JULES

The Joint UK Land Environment Simulator (JULES) is the UK community land surface model (Best et al., 2011;Clark et al., 2011) and the land surface scheme for the Hadley Centre climate model. It is closely based on the MOSES-TRIFFID land surface scheme (Cox, 2001), which was used in some of the first studies that predicted 'die-back' of the Amazon region. This study utilized version 2.1 of JULES. JULES simulates five PFTs: broadleaf trees, needleleaf trees, shrubs, C3 grasses and C4 grasses, which compete with each other following Lotka-Volterra dynamics (Cox 2001). Over Amazonia, broadleaf trees are the dominant plant functional type. In our simulations, a four-layer soil model is simulated with a total depth of 10 m, although individual plant functional types differ in their rooting depth. Net leaf photosynthesis is calculated based on Collatz et al. (Collatz et al., 1991;Collatz et al., 1992). Leaf photosynthesis is coupled to stomatal conductance through the leaf internal CO_2 concentration, calculated using the approach of Jacobs (1994). Leaf photosynthesis is scaled to canopy level using a multi-layer approach which adopts the 2-stream approximation of radiation interception from Sellers (1985). JULES simulates 3 vegetation pools (foliage, roots and wood), with maintenance respiration for each pool calculated dependent on tissue temperature and nitrogen content. Carbon fluxes from JULES are accumulated and passed to the TRIFFID vegetation dynamics model every 10 days. NPP is partitioned into a fraction used for growth of existing vegetation and a fraction for 'spreading' (Clark et al. 2011), based on the leaf area index. Tree mortality is not explicitly considered in the model. Biomass losses occur via turnover of carbon pools, each with specific turnover times, and prescribed large-scale disturbance rates.

INLAND

The Integrated Model of Land Surface Processes (INLAND) is the land surface module currently under development for the Brazilian Earth System Model, within the Brazilian scientific community (Costa et al. in prep.). It is originally based on IBIS model (Foley et al., 1996;Kucharik et al., 2000), and further adapted with special focus on the representation of tropical ecosystems of South America. INLAND simulates 12 different PFTs competing for available resources within the grid cell and the relative success of each PFT determines its fractional coverage. The model allows trees and herbaceous plants or grasses to experience different light and water availability: while trees in the upper canopy have priority to capture available light (thus shading the shrubs and grasses in the lower part of the canopy), the herbaceous plants are able to capture soil water first when it infiltrates the ground (Foley et al. 1996). INLAND uses the mechanistic treatment of canopy photosynthesis proposed by Farquhar et al. (1980) and the semi-mechanistic Ball-Berry approach to estimate stomatal conductance (Ball et al., 1987;Collatz et al., 1991;Collatz et al., 1992), computing gross photosynthesis, maintenance respiration and growth respiration to yield the annual carbon balance for each PFT. The vegetation dynamics module simulates biomass changes for each PFT on a yearly time step. Net primary productivity (NPP) is allocated to individual biomass pools (leaves, roots, wood) according to fixed allocation coefficients. Mortality is not explicitly modelled. Instead, biomass losses occur via turnover of the existing carbon pool, according to fixed turnover rates as well as via large-scale disturbance caused by fire or land use change.

4) Modelling protocol for the DGVM simulation runs

Model runs were performed based on the standardized Moore Foundation Andes-Amazon Initiative (AAI) modelling protocol (Zhang *et al.* 2015). To derive pre-industrial equilibrium of carbon pools and vegetation

distribution, the models were run through a 500 year spin-up period by repeating 39 years of bias-corrected NCEP climatology (Sheffield, Goteti & Wood 2006) with pre-industrial atmospheric CO_2 concentration of 278 ppm and for the transient runs with increasing CO_2 concentrations from Zhang *et al.* (2015).

5) Descritption of allometric equations and conversion of inventory data

Mitchard et al. (2014) provide AGB values (in Mg ha^{-1}) calculated with six different biomass equations (see Table S1) taking into account two (diameter-at-breast-height (DBH) and tree height) or three (DBH, height, wood density) parameters by using basin-wide or region-specific tree-height models and stem-level wood density (mean or derived from species data). From the efforts of the TEAM, RAINFOR and ATDM projects, measurements from 413 plots across the Amazon region are available (Lopez-Gonzalez et al., 2011;Lopez-Gonzalez et al., 2014). Plot measurements were taken from 1956 to 2013.

Additionally, we use data from Brienen et al. (2015) who provide values for WP and woody loss (WL) in Mg ha^{-1} from 321 plots.

In order to compare measured and modelled biomass, both variables need to match in terms of units. We convert the measured dry biomass of AGB and WP (in Mg dry matter (DM) ha^{-1} and Mg DM ha^{-1} yr^{-1}, respectively) to carbon mass (in MgC ha^{-1} and MgC ha^{-1} yr^{-1}). For this conversion, Martin and Thomas (2011) suggest a value of 0.474 gC/gDM, which we apply within our study. Martin and Thomas (2011) give a standard error of 0.025 gC/gDM or about 5.2% for their estimate of carbon content in dry matter.

Table S1: Description of the six allometric equations applied to calculate AGB of the inventory data used here, according to Mitchard et al. (2014) and Lopez-Gonzalez et al. (2014). To derive biomass from the measurements, the "Chave Moist equation" (Chave et al., 2005) for moist forests was used, which can have either three or two parameters, the latter one excluding tree height. "D" stands for diameter (DBH is diameter at breast height). "H" denotes tree height and indicates that AGB was calculated based on height estimated from DBH individually for each stem. "ρ" is wood density and indicates that values estimated for each stem were used to calculate AGB.

Abbreviation	Height model	Wood density	Explanation
$K_{DH\rho}$	Region-specific	Species-level	AGB calculated using the three parameter moist tropical forest model from Chave et al. (2005), where tree height is estimated from DBH individually for each stem based on the region-specific Weibull models from Feldpausch et al. (2012). Wood density is estimated for each stem using the mean value for the species in the Global Wood Density Database (Chave et al., 2009; Zanne et al., 2009), or the mean for the genus using congeneric taxa from Mexico, Central America and tropical South America if no data were available for that species (Mitchard et al. 2014). **This is the principal AGB dataset in Mitchard et al. (2014) and evaluated in our study in more detail.**
K_{DH}	Region-specific	Mean	AGB calculated using the three parameter moist tropical forest model from Chave et al. (2005) as above **but with a dataset mean wood density value of 0.63 applied to every stem.**
$K_{D\rho}$	Basin-wide	Species-level	AGB calculated using the three parameter moist tropical forest model from Chave et al. (2005) **but with**

			the pan-AmazonWeibull model from Feldpausch et al. (2012).
K_D	Basin-wide	Mean	AGB calculated with the pan-Amazonian height model and mean wood density applied to every stem.
$K_{2pD\rho}$	-	Species-level	AGB calculated using the two parameter moist tropical forest model from Chave et al. (2005), which excludes height. Wood density is estimated for each stem as described above.
K_{2pD}	-	Mean	AGB calculated using the two parameter moist tropical forest model from Chave et al. (2005), which excludes height. For wood density, the mean wood density value of 0.63 is applied to every stem.

Results

1) AGB maps for the remaining five allometric equations

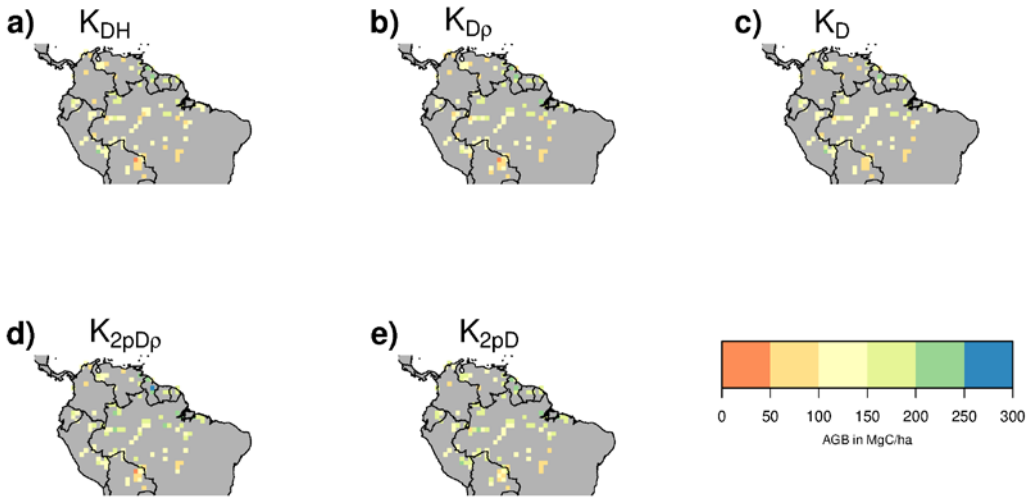

Figure S1: Maps of mean aboveground biomass (AGB) from inventory data within the simulated pixels derived from six allometric equations. The map for the principle AGB dataset calculated with allometric equation $K_{DH\rho}$ is shown in the main text.

2) Regional variability of within-pixel variability

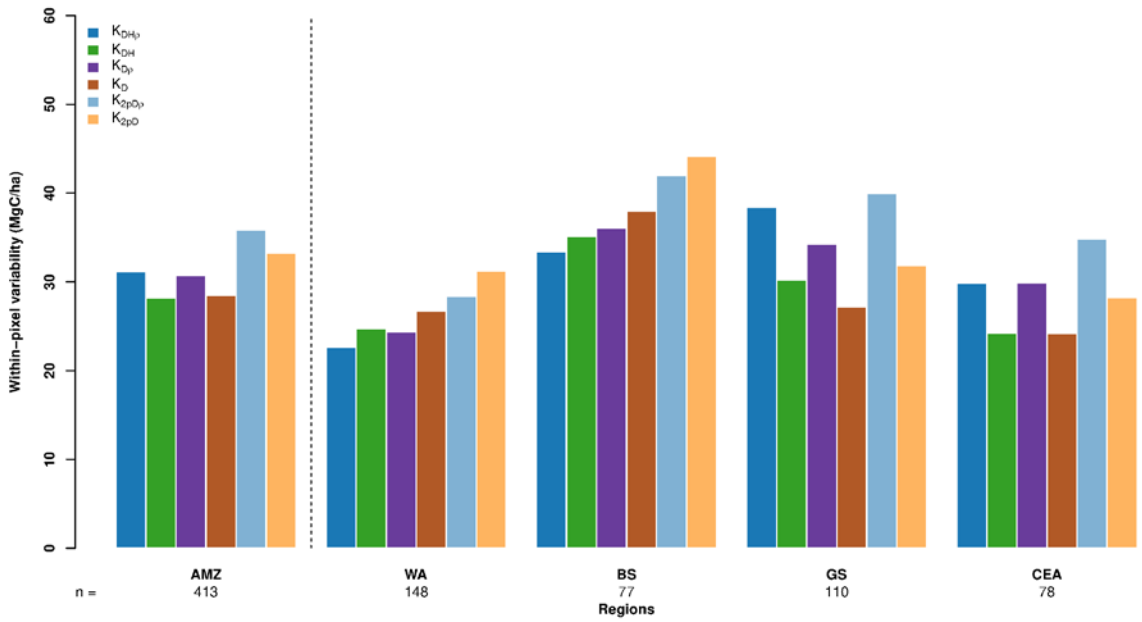

Figure S2: Regional variability of within-pixel variability σ_ε according to the Feldpausch regions (Feldpausch et al., 2011) for the different allometric equations (see Table S1). AMZ denotes the variability across the whole Amazon basin (and is used in our calculations). WA = Western Amazonia, BS = Brazilian Shield, GS = Guiana Shield, CEA = Central Eastern Amazon.

3) Mean aboveground biomass (AGB) for different allometric equations

Table S2: Values for observed mean aboveground biomass (AGB) for six different allometric equations.

Observed AGB Allometric equations	Mean $\bar{x}$ (MgC/ha)	Mean global variability σ_x (MgC/ha)	Within-pixel variability σ_ε (MgC/ha)	Corrected global variability $\sigma_{x,corr}$ (MgC/ha)	Max. achievable correlation r_{max}
$K_{DH\rho}$	135.96	49.80	31.14	38.86	0.78
K_{DH}	134.76	41.04	28.20	29.82	0.72
$K_{D\rho}$	134.66	42.45	30.73	29.29	0.69
K_{D}	134.19	35.94	28.44	21.97	0.61
$K_{2pD\rho}$	153.14	49.25	35.84	33.78	0.68
K_{2pD}	152.62	41.95	33.25	25.58	0.61

Table S3: Comparison metrics for AGB.

AGB		INLAND	JULES	ORCHIDEE	LPJmL
Mean $\bar{y}$ (MgC/ha)		114.36	151.33	217.60	169.92
Mean global variability σ_y (MgC/ha)		32.78	13.39	61.96	54.00
Mean bias ($\bar{y}/\bar{x}$)	$K_{DH\rho}$	0.84	1.12	1.60	1.25
	K_{DH}	0.85	1.12	1.61	1.26
	$K_{D\rho}$	0.85	1.12	1.62	1.26
	K_{D}	0.85	1.12	1.62	1.26
	$K_{2pD\rho}$	0.75	0.99	1.42	1.11
	K_{2pD}	0.75	0.99	1.42	1.11
Pattern amplitude ($\sigma_y/\sigma_{x,corr}$)	$K_{DH\rho}$	0.86	0.35	1.62	1.43
	K_{DH}	1.12	0.45	2.11	1.86
	$K_{D\rho}$	1.14	0.46	2.15	1.88
	K_{D}	1.55	0.62	2.91	2.55
	$K_{2pD\rho}$	0.99	0.40	1.87	1.63
	K_{2pD}	1.33	0.54	2.50	2.19
Similarity of pattern (r_{corr})	$K_{DH\rho}$	0.46	0.42	0.53	0.25
	K_{DH}	0.55	0.49	0.54	0.36
	$K_{D\rho}$	0.48	0.43	0.56	0.21
	K_{D}	0.59	0.53	0.56	0.36
	$K_{2pD\rho}$	0.47	0.43	0.56	0.21
	K_{2pD}	0.58	0.52	0.55	0.34

Table S4: Mean simulated values for woody productivity (WP) and woody residence time (τ) calculated only for pixels that contain observational plots.

WP	**INLAND**	**JULES**	**ORCHIDEE**	**LPJmL**
Mean $\bar{y}$ (MgC/ha/yr)	8.01	5.18	9.14	4.47
Mean variability σ_y (MgC/ha/yr)	1.09	0.72	1.60	0.75
τ	**INLAND**	**JULES**	**ORCHIDEE**	**LPJmL**
Mean $\bar{y}$ (years)	14.73	31.03	25.79	34.68
Mean variability σ_y (years)	3.15	5.66	5.79	8.45

Supplementary Literature

Ball, J. T., Woodrow, I. E., and Berry, J. A.: A model predicting stomatal conductance and its contribution to the control of photosynthesis under different environmental conditions., in: Progress in Photosynthesis Research, edited by: Biggens, J., Springer, The Netherlands, 221-224, 1987.

Best, M. J., Pryor, M., Clark, D. B., Rooney, G. G., Essery, R. L. H., Ménard, C. B., Edwards, J. M., Hendry, M. A., Porson, A., Gedney, N., Mercado, L. M., Sitch, S., Blyth, E., Boucher, O., Cox, P. M., Grimmond, C. S. B., and Harding, R. J.: The Joint UK Land Environment Simulator (JULES), model description – Part 1: Energy and water fluxes, Geosci. Model Dev., 4, 677-699, 10.5194/gmd-4-677-2011, 2011.

Bondeau, A., Smith, P. C., Zaehle, S., Schaphoff, S., Lucht, W., Cramer, W., Gerten, D., Lotze-Campen, H., Müller, C., Reichstein, M., and Smith, B.: Modelling the role of agriculture for the 20th century global terrestrial carbon balance, Global Change Biology, 13, 679-706, 2007.

Chave, J., Andalo, C., Brown, S., Cairns, M. A., Chambers, J. Q., Eamus, D., Fölster, H., Fromard, F., Higuchi, N., Kira, T., Lescure, J. P., Nelson, B. W., Ogawa, H., Puig, H., Riéra, B., and Yamakura, T.: Tree allometry and improved estimation of carbon stocks and balance in tropical forests, Oecologia, 145, 87–99, 2005.

Clark, D. B., Mercado, L. M., Sitch, S., Jones, C. D., Gedney, N., Best, M. J., Pryor, M., Rooney, G. G., Essery, R. L. H., Blyth, E., Boucher, O., Harding, R. J., Huntingford, C., and Cox, P. M.: The Joint UK Land Environment Simulator (JULES), model description – Part 2: Carbon fluxes and vegetation dynamics, Geosci. Model Dev., 4, 701-722, 10.5194/gmd-4-701-2011, 2011.

Collatz, G. J., Ball, J. T., Grivet, C., and Berry, J. A.: Physiological and environmental regulation of stomatal conductance, photosynthesis and transpiration: a model that includes a laminar boundary layer, Agricultural and Forest Meteorology, 54, 107-136, 1991.

Collatz, G. J., Ribas-Carbo, M., and Berry, J. A.: Coupled photosynthesis-stomatal conductance model for leaves of C4 plants. , Functional Plant Biology, 19, 519-538, 1992.

Cox, P. M.: Description of the TRIFFID Dynamic Global Vegetation Model, Hadley Centre, Met Office, UK, 16, 2001.

Cressie, N.: Statistics for spatial data, John Wiley & Sons, New York, 1993.

Delbart, N., Ciais, P., Chave, J., Viovy, N., Malhi, Y., and Le Toan, T.: Mortality as a key driver of the spatial distribution of aboveground biomass in Amazonian forest: results from a dynamics vegetation model. , Biogeosciences, 7, 3017-3039, 2010.

Ducoudré, N., Laval, K., and Perrier, A.: SECHIBA, a new set of parameterizations of the hydrologic exchanges at the land-atmosphere interface within the LMD atmospheric general circulation model., Journal of Climate, 6, 248-273, 1993.

Farquhar, G. D., von Caemmerer, S., and Berry, J. A.: A biochemical model of photosynthesic CO_2 assimilation in leaves of C3 plants, Planta, 149, 78-90, 1980.

Farquhar, G. D., and von Caemmerer, S.: Modelling of photosynthetic response to environmental conditions. , in: Physiological plant ecology II, Springer, Berlin, Heidelberg, 549-587, 1982.

Feldpausch, T. R., Banin, L., Phillips, O. L., Baker, T. R., Lewis, S. L., Quesada, C. A., Affum-Baffoe, K., Arets, E. J. M. M., Berry, N. J., Bird, M., Brondizio, E. S., de Camargo, P., Chave, J., Djagbletey, G., Domingues, T. F., Drescher, M., Fearnside, P. M., França, M. B., Fyllas, N. M., Lopez-Gonzalez, G., Hladik, A.,

Higuchi, N., Hunter, M. O., Iida, Y., Salim, K. A., Kassim, A. R., Keller, M., Kemp, J., King, D. A., Lovett, J. C., Marimon, B. S., Marimon-Junior, B. H., Lenza, E., Marshall, A. R., Metcalfe, D. J., Mitchard, E. T. A., Moran, E. F., Nelson, B. W., Nilus, R., Nogueira, E. M., Palace, M., Patiño, S., Peh, K. S. H., Raventos, M. T., Reitsma, J. M., Saiz, G., Schrodt, F., Sonké, B., Taedoumg, H. E., Tan, S., White, L., Wöll, H., and Lloyd, J.: Height-diameter allometry of tropical forest trees, Biogeosciences, 8, 1081-1106, 10.5194/bg-8-1081-2011, 2011.
Foley, J. A., Prentice, I. C., Ramankutty, N., Levis, S., Pollard, D., Sitch, S., and Haxeltine, A.: An integrated biosphere model of land surface processes, terrestrial carbon balance, and vegetation dynamics, Global Biogeochemical Cycles, 10, 1996.
Gerten, D., Schaphoff, S., Haberlandt, U., Lucht, W., and Sitch, S.: Terrestrial vegetation and water balance - hydrological evaluation of a dynamic global vegetation model, Journal of Hydrology, 286, 249-270, 2004.
Guimberteau, M., Drapeau, G., Ronchail, J., Sultan, B., Polcher, J., Martinez, J. M., Prigent, C., Guyot, J. L., Cochonneau, G., Espinoza, J. C., Filizola, N., Fraizy, P., Lavado, W., De Oliveira, E., Pombosa, R., Noriega, L., and Vauchel, P.: Discharge simulation in the sub-basins of the Amazon using ORCHIDEE forced by new datasets, Hydrol. Earth Syst. Sci., 16, 911-935, 10.5194/hess-16-911-2012, 2012.
Jacobs, C.: Direct impact of atmospheric CO2 enrichment on regional transpiration., PhD thesis, Wageningen Agricultural University., Wageningen, 1994.
Johnson, M. O., Galbraith, D., Gloor, M., De Deurwaerder, H., Guimberteau, M., Rammig, A., Thonicke, K., Verbeeck, H., Von Randow, C., and al., e.: Variation in stem mortality rates determines patterns of above-ground biomass in Amazonian forests: implications for dynamic global vegetation models, Global Change Biology, 22, 3996-4013, doi: 10.1111/gcb.13315, 2016.
Krinner, G., Viovy, N., de Noblet-Ducoudre, N., Ogee, J., Polcher, J., Friedlingstein, P., Ciais, P., Sitch, S., and Prentice, I. C.: A dynamic global vegetation model for studies of the coupled atmosphere biosphere system, Global Biogeochemical Cycles, 19, GB1015, 2005.
Kucharik, C. J., Foley, J. A., Delire, C., Fisher, V. A., Coe, M. T., Lenters, J. D., Young-Molling, C., and Ramankutty, N.: Testing the performance of a dynamic global ecosystem model: water balance, carbon balance, and vegetation structure, Global Biogeochemical Cycles, 14, 795-825, 2000.
Lopez-Gonzalez, G., Lewis, S., Burkitt, M., and Phillips, O.: ForestPlots.net: a web application and research tool to manage and analyse tropical forest plot data, Journal of Vegetation Science, 22, 610-613, 2011.
Martin, A. R., and Thomas, S. C.: A Reassessment of Carbon Content in Tropical Trees, PLoS ONE, 6, e23533, 10.1371/journal.pone.0023533, 2011.
Ruimy, A., Dedieu, G., and Saugier, B.: TURC: A diagnostic model of continental gross primary productivity and net primary productivity. , Global Biogeochemical Cycles, 10, 269-285, 1996.
Sellers, P. J.: Canopy reflectance, photosynthesis and transpiration., International Journal of Remote Sensing, 6, 1335-1372, 1985.
Sitch, S., Smith, B., Prentice, I. C., Arneth, A., Bondeau, A., Cramer, W., Kaplans, J. O., Levis, S., Lucht, W., Sykes, M. T., Thonicke, K., and Venevsky, S.: Evaluation of ecosystem dynamics, plant geography and terrestrial carbon cycling in the LPJ dynamic global vegetation model, Global Change Biology, 9, 161-185, 2003.
Taylor, K. E.: Summarizing multiple aspects of model performance in a single diagram, Journal of Geophysical Research, 106, 7183-7192, 2001.
Thonicke, K., Venevsky, S., Sitch, S., and Cramer, W.: The role of fire disturbance for global vegetation dynamics: coupling fire into a dynamic global vegetation model, Global Ecology and Biogegraphy, 10, 661-677, 2001.
Zhang, Y., and Lei Cheng, H.: Some new deformation formulas about variance and covariance., Proceedings of 4th International Conference on Modelling, Identification and Control(ICMIC2012), 987–992, 2012.